Performance of GFDM over Frequency-Selective Channels

Bruno M. Alves, Luciano Leonel Mendes, Dayan Adionel Guimarães & Ivan Simões Gaspar

***Abstract*— The advent of Analog Television Switch-off will introduce new possibilities for wireless Internet services in UHF bands. Cognitive Radios are devices that are able to dynamically access the vacant TV channels, without causing severe interference to the incumbents. This technology is being proposed for the next generation of mobile communication systems. Cognitive Radio Networks will allow for a better spectral occupancy of these new communication opportunities in the UHF bands. GFDM is a flexible multi-carrier transmission technique that allows for controlling the out-of-band emissions and the PAPR, which are the major drawbacks of OFDM, technology that is current being proposed as aerial interface of the next generation of mobile communication system. The aim of this paper is to present the foundations of GFDM and analyze its performance over frequency-selective channels, comparing it with OFDM. Simulation results are validated by theoretical curves, which allows one to conclude that the theoretical approximations proposed for OFDM can also be used to estimate the performance of GFDM.**

***Index Terms*— GFDM, Frequency-Selective Channel, Performance.**

I. Introduction

The demand for high data rate in mobile communication systems has severely increased in the last years [1]. The opportunistic utilization of white spaces [2] is a solution that can be used to attend this demand, mainly in the UHF (Ultra High Frequency) bands [3] after the ATSO (Analog Television Switch-Off) [4]. Several countries are planning the ATSO and they consider reorganizing the allocation of Digital Television channels in order to release part of the UHF spectrum for mobile communication. This available spectrum, which is known as digital dividend [5], can be efficiently used by the Cognitive Radio (CR) technology [6].

In a CR network, radio terminals can sense the spectrum to detect white spaces, establishing the communication in a vacant channel. The radio terminals keep sensing the spectrum and, if a primary user is detected, they change their operation frequency to occupy another white space, avoiding harmful interference to the primary user. The CR concept was proposed by Joseph Mitola III in 1999 [7] and it is being considered for the next generations of digital wireless communication standards, such as IEEE 802.22 [8], IEEE 802.16h [9], IEEE 802.11af [10] and LTE Advanced [11].

Manuscript received in July 1st 2013; reviewed in XXXXX YYth 2013.

B. M. Alves (alves.bm@gmail.com), L. L. Mendes (luciano@inatel.br and D. A. Guimarães (dayan@inatel.br) are with Instituto Nacional de Telecomunicações - Inatel. Av. João de Camargo, 510 - Santa Rita do Sapucaí - MG - Brasil - 37540-000. I. S. Gaspar (ivan.gaspar@ifn.et.tu-dresden.de) is with Technische Universität Dresden - T. U. Dresden, Georg-Schumann-Str. 11, D-01187 Dresden, Germany.

Interference from opportunistic users in primary users is a key issue for the CR technology. Signals from CR terminals cannot reduce the performance of primary users. Besides spectrum sensing techniques [12] [13] [14], which play an important role to avoid interference to the primary users, the digital modulation scheme is a very important issue in this context. Most of modern digital communication standards use OFDM (Orthogonal Frequency Division Multiplexing) [15] as the air interface, because of its flexibility and robustness in frequency-selective channels. Nevertheless, OFDM presents some drawbacks that affect its application specially in CR systems. Among these drawbacks there are the high out-of-band emission [16] and the high PAPR (Peak-to-Average Power Ratio) [17]. Out-of-band emissions are caused by the rectangular pulse shape of the filter used in the transmitter and the high PAPR is caused by the random sum of several in-phase subcarriers. There are several papers in the literature proposing solutions to reduce the PAPR [17] [18] [19] [20] and the out-of-band-emissions; see [21] and references therein.

In [22] the authors present a multi-carrier transmission technique that is more suitable for CR operation because it reduces the out-of-band emissions and allows for controlling the PAPR. This technique is called GFDM (Generalized Frequency Division Multiplexing) [22] [23] [24] [25], which can be seen as a generalization of OFDM [26]. The main difference between GFDM and OFDM is that GFDM transmits $M\dot{K}$ data symbols per frame using M time-slots with K subcarriers, where each data symbol is represented by a pulse shape $g(t)$, whereas OFDM transmits K data symbols using one time-slot with K subcarriers, where each symbol is represented by a rectangular pulse shape. This means that GFDM can model the spectrum shape by choosing the appropriate pulse shape $g(t)$. Moreover, the frequency spacing between subcarriers is more flexible in GFDM than in OFDM, and the low out-of-band emission in GFDM allows for a higher flexibility for spectrum fragmentation.

GFDM can achieve higher spectrum efficiency because it does not need to use virtual subcarriers to avoid adjacent channel interference and because it reduces the ratio between the guard time interval [15] and the total frame duration. The main drawbacks of GFDM are ICI (Inter-carrier Interference) [27] and higher complexity. However, efforts are being made to reduce the complexity of the system and to obtain models that are suitable for hardware implementation [23]. Additionally, ICI-cancelling techniques can increase the performance of GFDM. In fact, DSIC (Double Sided ICI Cancelling) [28] can reduce the BER (Bit Error Rate) of GFDM in AWGN (Additive White Gaussian Noise) channels to the same BER level achieved by OFDM.

The aim of this paper is to present the analysis of the performance of GFDM in frequency-selective channels considering different channel profiles. To the best of the authors' knowledge, this is a novel analysis and, thereby, it is the main contribution of this paper. Three types of receivers are considered: ZFR (Zero Forcing Receiver), MFR (Matched Filter Receiver) and Matched Filter Receiver with DSIC (MFR-DSIC). All results are compared with the performance of an OFDM system. All simulation results that have been obtained using Matlab are compared with theoretical curves, which allow one to conclude that the symbol error probability expression proposed for OFDM can be used to estimate the performance of GFDM.

The remaining of this paper is organized as follows: Section II presents the generation of GFDM symbols, whereas Section III presents three techniques used to recover the transmitted information. Section IV contains the performance analysis of GFDM considering AWGN and Section V evaluates the performance over frequency-selective channels. Finally, Section VI concludes the paper.

II. Generation of the GFDM Signal

GFDM is a flexible multi-carrier modulation scheme that has been introduced by Fettweis et al [22] and it has interesting features for CR applications. Figure 1 depicts the block diagram of the GFDM transmitter.

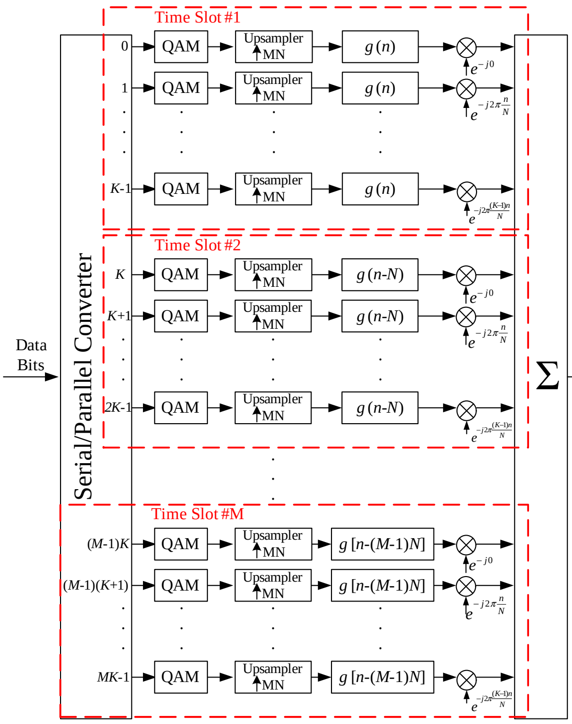

Fig. 1. Block diagram of the GFDM transmitter.

The input bits are converted into MK data streams that feed MK independent J-QAM mappers. Each mapper converts a block of q bits into a data symbol $s_{k,m}$, $k = 0, 1, 2, \ldots, K-1$, $m = 0, 1, 2, \ldots, M-1$. Therefore, each of the K subcarriers transmits M data symbols per GFDM frame. Since the mappers are independent, different constellation orders can be used in each stream, allowing for dynamic bit loading mapping according to the channel conditions for each subcarrier [29]. Because GFDM transmits M data symbols in each subcarrier using M time-slots, the data symbols can be organized in a frame structure given by

$$\mathbf{S} = \begin{bmatrix} s_{0,0} & s_{0,1} & s_{0,2} & \cdots & s_{0,M-1} \\ s_{1,0} & s_{1,1} & s_{1,2} & \cdots & s_{1,M-1} \\ s_{2,0} & s_{2,1} & s_{1,2} & \cdots & s_{2,M-1} \\ \vdots & \vdots & \vdots & \ddots & \vdots \\ s_{K-1,0} & s_{K-1,1} & s_{K-1,2} & \cdots & s_{K-1,M-1} \end{bmatrix}, \tag{1}$$

where the k-th row represents the symbols transmitted in the k-th subcarrier and the m-th column represents the symbols transmitted in the m-th time-slot.

Each data symbol $s_{k,m}$ is up-sampled by zero-padding $MN-1$ zeroes, resulting in the sequence

$$s_{k,m}(n) = s_{k,m}\delta(n - mN), \tag{2}$$

where N is the number of samples used to represent a time-slot. This sequence is applied to a transmit filter with impulse response $g(n)$ of length $L = MN$. If conventional linear convolution is used, like in the Filter Bank Multi-carrier (FBMC) [30] schemes, the guard time interval between the GFDM frames should be larger than the channel delay spread plus the filter spreading in order to avoid IFI (Inter Frame Interference), as depicted in Figure 2 for $N = 8$, $M = 3$ and an arbitrary impulse response $g(n)$. Such a large guard time interval would be a considerable drawback, causing throughput reduction, leading to a poor spectrum efficiency. However, this problem can be easily avoided by using a technique called tail-biting [22]. In this technique, the mN last samples at the output of the filter are shifted to the first mN positions, as illustrated in Figure 3. This process can be made by circular convolution [31].

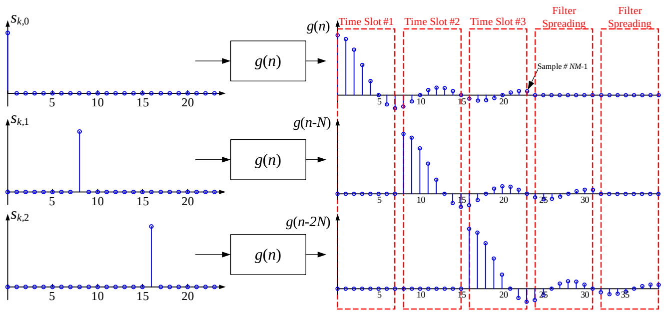

Fig. 2. GFDM symbol obtained by linear convolution.

In order to use the tail-bitting technique, the filter impulse response must allow for circular shifts of N samples, as shown in Figure 3 [22] [23].

Since $g(n)$ can have non-rectangular pulse shape, GFDM subcarriers can be non orthogonal to each other, which can lead to ICI. Additionally, the transmit filter impulse response can cause ISI (Intersymbol Interference) among the M data

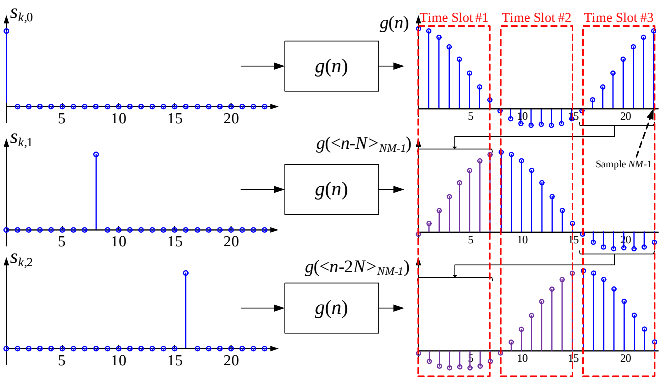

Fig. 3. GFDM symbol obtained by circular convolution.

symbols transmitted in a given subcarrier. In [26], the author presents a deep analysis about the influence of Raised Cosine (RC) and Root Raised Cosine (RRC) filters in the performance of GFDM systems. The impact of the roll-off factor is analyzed as well. The major conclusions of this analysis are: i) if RCs are used on the transmitter and receiver sides there will be larger ISI when compared with the use of RRC because the Nyquist criterion is not satisfied, however the ICI will be smaller than the one obtained with RRC because of the sharper frequency response of the RC and; ii) the smaller the roll-off factor the better the system performance because of the reduction of the ICI. Clearly there is a trade-off between ISI and ICI in the choice of the RC or RRC.

Once the filter impulse response is chosen, each sub-stream is up-converted by a complex subcarrier given by

$$p_k(n) = e^{-j2\pi k \frac{n}{N}}. \tag{3}$$

At this point, it is important to notice that in GFDM the frequency spacing between two adjacent subcarriers is not dependent of the number of subcarriers, K, as in OFDM, but it depends on the number of samples representing a time-slot, N. Notice that $N \geq K$ to avoid aliasing [31], which means that it is possible to increase the sampling rate by increasing the length of $g(n)$.

From Figure 1 it is possible to conclude that the GFDM signal, without the guard time interval, is given by

$$x(n) = \sum_{m=0}^{M-1} \sum_{k=0}^{K-1} s_{k,m}(n) \circledast g\left(< n - mN >_{NM-1}\right) p_k(n), \tag{4}$$

where $< \cdot >_N$ denotes the modulo operator and $\circledast$ denotes the circular convolution. Since $s_{k,m}(n)$ is a discrete delta function with amplitude $s_{k,m}$, as defined in (2), Eq. (4) can be rewritten as

$$x(n) = \sum_{m=0}^{M-1} \sum_{k=0}^{K-1} s_{k,m} g_m(n) p_k(n), \tag{5}$$

where

$$g_m(n) = g\left(< n - mN >_{NM-1}\right). \tag{6}$$

It is possible to express (5) in the following matrix form:

$$\mathbf{x} = \operatorname{diag}\left(\mathbf{PSG}\right), \tag{7}$$

where diag$(\cdot)$ returns the main diagonal of a matrix,

$$\mathbf{P} = \left[\begin{array}{cccc} p_0(n)^T & p_1(n)^T & \cdots & p_{k-1}(n)^T \end{array}\right] \tag{8}$$

is the matrix containing K complex subcarriers and

$$\mathbf{G} = \left[\begin{array}{c} g_0(n) \\ g_1(n) \\ g_2(n) \\ \vdots \\ g_{M-1}(n) \end{array}\right] \tag{9}$$

is the matrix containing M circular-shifted versions of $g(n)$.

Taking the appropriate matrix operations it is possible to represent the GFDM signal as

$$\mathbf{x} = \mathbf{Ad}, \tag{10}$$

where

$$\mathbf{d} = \left[\begin{array}{c} s_{0,0} \\ s_{1,0} \\ \vdots \\ s_{K-1,0} \\ s_{0,1} \\ s_{1,1} \\ \vdots \\ s_{K-1,M-1} \end{array}\right] \tag{11}$$

is the serialized symbol vector and

$$\mathbf{A} = \left[\begin{array}{c} g_0(n)p_0(n) \\ g_0(n)p_1(n) \\ \vdots \\ g_0(n)p_{K-1}(n) \\ g_1(n)p_0(n) \\ \vdots \\ g_{M-1}(n)p_{K-1}(n) \end{array}\right]^T \tag{12}$$

is the transmission matrix.

Eq. (10) is an important representation of the GFDM signal because it will allow a clear interpretation of the reception chain, as discussed in the next section.

Another important difference between OFDM and GFDM is the insertion of the guard time interval. Both schemes employs the cyclic prefix (CP) [15] to avoid IFI (Inter-frame Interference). However, while OFDM requires a CP between two time-slots, GFDM requires a CP only between GFDM frames, since the interference between time-slots are avoided by the appropriate choice of the pulse shape $g(n)$. Figure 4 shows the CP insertion in both systems.

Since the CP length must be the same in both cases, GFDM achieves a higher spectrum efficiency when compared with OFDM. The OFDM bit rate is given by

$$R_O = \frac{K}{T + T_{CP}} \log_2(J), \tag{13}$$

where T is the duration of one time-slot and T_{CP} is the duration of the cyclic prefix, while GFDM bit rate is given by

$$R_G = \frac{KM}{MT + T_{CP}} \log_2(J). \tag{14}$$

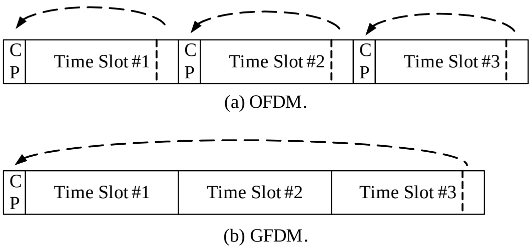

Fig. 4. Insertion of Cyclic Prefix. (a) OFDM signal. (b) GFDM signal.

The spectral efficiency gain of GFDM over OFDM is given by

$$\rho = \frac{R_G}{R_O} = \frac{1+\frac{T_{CP}}{T}}{1+\frac{T_{CP}}{MT}}. \tag{15}$$

Since channel delay profiles for Wireless Regional Area Networks (WRAN) applications may have delay spreads of up $60\mu s$ [32], which requires a large CP, the possibility of using only one CP for several time-slots becomes an interesting advantage of GFDM, when compared with OFDM.

III. Reception of the GFDM Signal

Figure 5 shows the basic block diagram of a GFDM receiver.

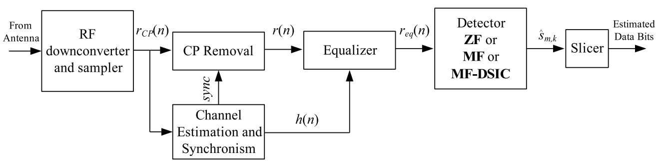

Fig. 5. Basic block diagram of a GFDM receiver.

The signal from the antenna is down-converted to base-band and sampled, resulting in the discrete received signal $r_{CP}(n)$. In this paper a time-invariant multipath channel with impulse response $h(n)$ has been considered, leading to

$$r_{CP}(n) = x_{CP}(n) * h(n) + w(n) \tag{16}$$

where $x_{CP}(n)$ is the transmitted signal with the cyclic prefix and $w(n)$ is a vector of gaussian noise samples with zero mean and variance σ_n^2.

The received signal is used for synchronization and to estimate the channel impulse response. Subsequently, the CP is removed. It is assumed that the CP length is larger than the channel delay spread, which means that there is no interference among GFDM frames.

Afterwards, the signal must be equalized to compensate for the influence of the channel frequency response in the received signal. The channel frequency response can be considered flat for each subcarrier if K is large enough to make the subcarriers bandwidth smaller than the channel coherence bandwidth. In this case, the received signal can be equalized in the frequency domain using an Zero-forcing equalizer. Assuming the receiver is able to estimate the channel impulse response, the equalized sequence can be obtained from

$$r_{eq}(n) = \text{IFFT}\left\{\frac{\text{FFT}\left[r(n)\right]}{\text{FFT}\left[h(n)\right]}\right\} \tag{17}$$

where $\text{FFT}(\cdot)$ is the Fast Fourier Transform and $\text{IFFT}(\cdot)$ is the Inverse Fast Fourier Transform.

The equalized sequence is applied into a detector. Three approaches will be exploited in this paper: ZFR, MFR and MFR-DSIC. More details about these approaches are presented in the next subsections. After detection, the Slicer uses the recovered symbols $\hat{s}_{k,m}$ to estimate the data bits.

A. Zero-forcing Receiver

The matrix representation of the GFDM signal in (10) allows one to conclude that the inverse of matrix $\mathbf{A}$ can be used to recover the data symbols, that is,

$$\hat{\mathbf{d}}_{\mathbf{ZF}} = \mathbf{A}^{-1}\mathbf{r}_{\mathbf{eq}}, \tag{18}$$

where $\hat{\mathbf{d}}_{\mathbf{ZF}}$ is the recovered vector using the zero-forcing approach, $\mathbf{A}^{-1}$ is the inverse of matrix $\mathbf{A}$ and $\mathbf{r}_{\mathbf{eq}}$ is the equalized signal vector.

Matrix $\mathbf{A}$ has order KM x NM, $N \geq K$, which means that it is not necessarily square. Therefore, the inversion operation may not be suitable for this matrix. In this case, it is possible to use the pseudoinverse matrix of $\mathbf{A}$, defined by

$$\mathbf{A}^{+} = \mathbf{A}^{H}\left(\mathbf{A}\mathbf{A}^{H}\right)^{-1}, \tag{19}$$

where $\mathbf{A}^H$ is the Hermitian (conjugate and transpose) matrix of $\mathbf{A}$. Notice that $\mathbf{A}^{+}\mathbf{A} = \mathbf{I}_{NM}$ where $\mathbf{I}_{NM}$ is the identity matrix of order NM.

The ZFR is capable of completely removing the ICI resulted from the non-orthogonality between the subcarriers. However, since $\mathbf{A}^{+}$ has high values, this procedure enhances the influence of the noise in the detected symbols, which increases the BER.

B. Matched Filter Receiver

The MFR can be seen as K parallel single frequency receivers processing the equalized signal $r_{eq}(n)$. Since only the time samples $n = mN$ are of interest, the MFR can be implemented as a correlator receiver [33], as shown in Figure 6.

The symbol received at a given subcarrier and at a given time-slot is

$$\hat{s}_{k',m'} = \sum_{n=0}^{NM-1} r_{eq}(n)\left[g_{m'}(n)p_{k'}(n)\right]^{*}. \tag{20}$$

If the influence of the noise and multipath channel is disregarded, then $r_{eq}(n) = x(n)$, which leads to

$$\hat{s}_{k',m'} = s_{k',m'} + \overbrace{\sum_{\substack{m=0\\m\neq m'}}^{M-1} s_{k',m} \sum_{n=0}^{NM-1} g_m(n)g^*_{m'}(n)}^{\text{ISI}} +$$
$$+ \overbrace{\sum_{\substack{k=0\\k\neq k'}}^{K-1} s_{k,m'} \sum_{n=0}^{NM-1} |g_{m'}(n)|^2 p_{k-k'}(n)}^{\text{ICI caused by symbols from the same time slot}} + \tag{21}$$
$$+ \overbrace{\sum_{\substack{m=0\\m\neq m'}}^{M-1} \sum_{\substack{k=0\\k\neg k'}}^{K-1} s_{k,m} \sum_{n=0}^{NM-1} g_m(n)g^*_{m'}(n)p_{k-k'}(n)}^{\text{ICI caused by symbols from other time slots}},$$

where

$$p_{k-k'}(n) = p_k(n)p^*_{k'}(n) = \mathrm{e}^{-j2\pi\frac{k-k'}{N}n}, \tag{22}$$

and where it has been considered that the transmit pulse has unitary energy.

Using the matrix representation (10) it is possible to perform the MFR process as

$$\hat{\mathbf{d}}_{\mathbf{MF}} = \mathbf{A}^H\mathbf{r}_{\mathbf{eq}}, \tag{23}$$

where $\hat{\mathbf{d}}_{\mathbf{MF}}$ is the recovered vector using the MFR.

Moreover, $\mathbf{A}^H\mathbf{A}$ can be used to evaluate the influence of the ISI and ICI in the received vector. Figure 7 shows the magnitude of the interference in the GFDM frame for $K = 16$, $M = 3$ and $N = K$. Notice that $g(n)$ is a RRC filter with roll-off 0.1 and 0.75 for Figures 7(a) and 7(b), respectively. The main diagonal of the matrix represented in Figure 7 is associated with the desired information and all other values in the matrix represents the interferences at the output of the MFR.

The conclusion that can be achieved from Figure 7 is that larger values of the roll-off factor result in larger ICI, decreasing the performance of the MFR. Therefore, the ISI in the GFDM frame can be minimized by choosing the appropriate filter impulse response, while the ICI can be reduced by using a smaller roll-off [26].

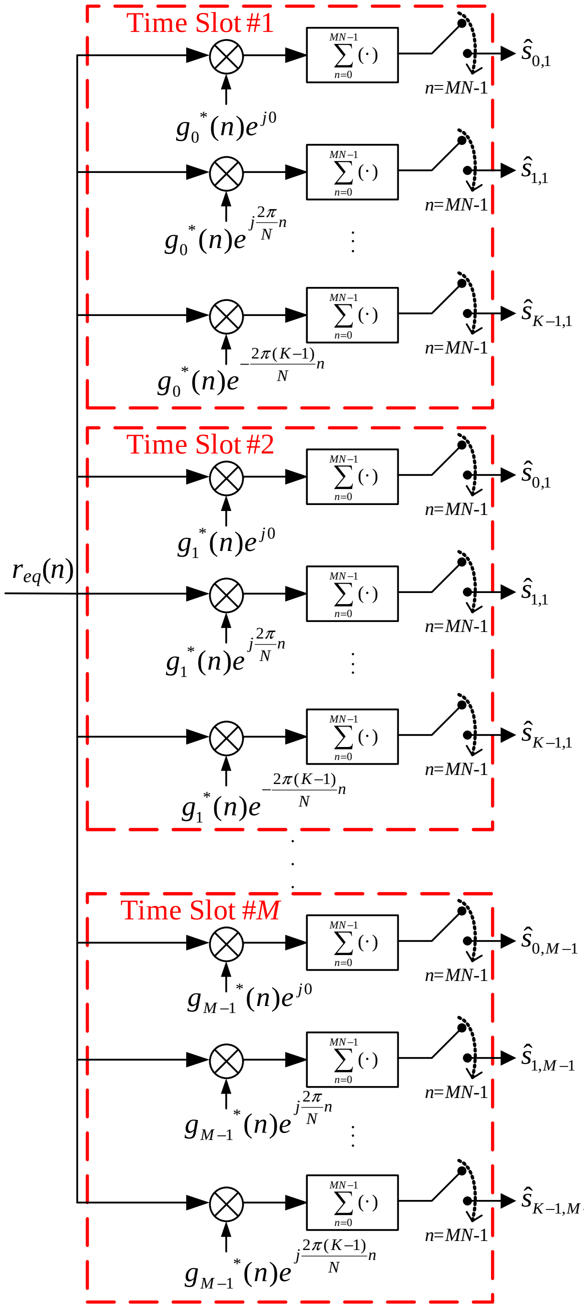

Fig. 6. Block diagram of MFR implemented as a correlator.

C. Matched Filter Receiver with DSIC

From Figure 7 it is possible to observe that one of the major source of interference at the output of the MFR is the ICI between adjacent subcarriers. This high ICI, which increases the BER, can be minimized by using the DSIC algorithm [34]. Figure 8 depicts the basic diagram of the DSIC. The basic idea of this technique is to subtract the ICI caused by the $(k+1)$-th and $(k-1)$-th subcarriers from the signal received at the k-th subcarrier. First, the equalized received sequence $r_{eq}(n)$ is applied to the MFR, resulting in the ICI-corrupted sequence $\hat{d}_{MF}(n)$. To eliminate the ICI from the signal received at the k-th subcarrier it is necessary to use the $2M$ samples from $\hat{d}_{MF}(n)$ corresponding to the data received at the $(k+1)$-th and $(k-1)$-th subcarriers during M times slots. A column vector with $MN-1$ zeros is created and the samples in the positions corresponding to subcarriers $k-1$ and $k+1$ for all time-slots are updated with the corresponding samples from $\hat{d}_{MF}(n)$. This procedure leads to

$$c(n) = \begin{cases} \hat{d}_{MF}(n) & \text{if } n = k \pm 1 + mK, \quad m = 0, \ldots, M-1 \\ 0 & \text{otherwise.} \end{cases} \tag{24}$$

The transmission matrix in (12) can be used to generate a GFDM frame carrying the ICI that interferes with the k-th subcarrier, i.e.,

$$\mathbf{v_k} = \mathbf{A}\mathbf{c}, \tag{25}$$

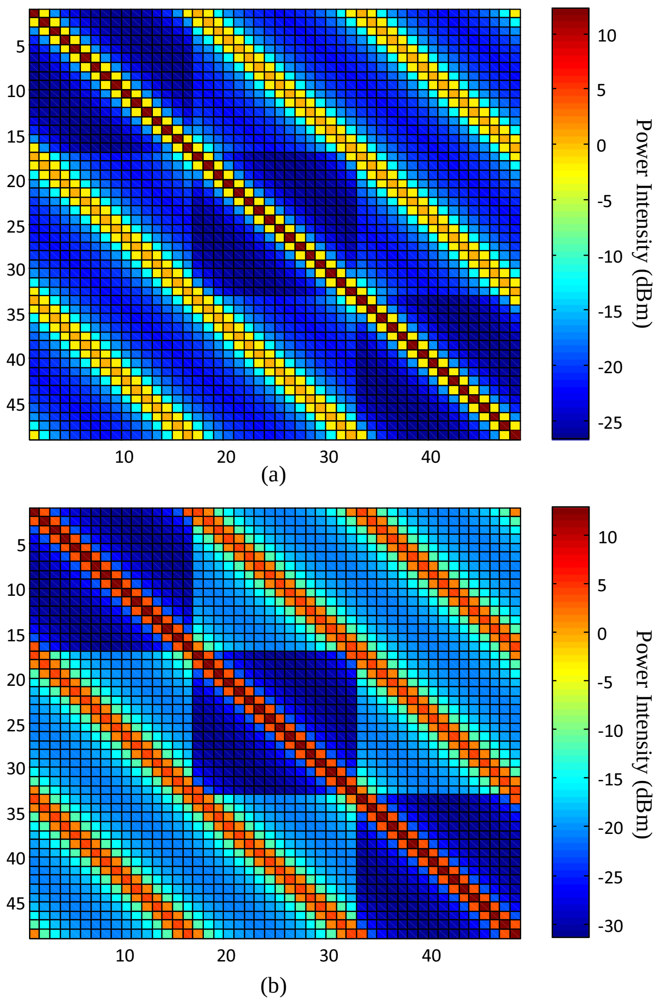

Fig. 7. Interference pattern at the output of a MFR. (a) $M = 3$, $K = 16$ and $\alpha = 0.1$. (b) $M = 3$, $K = 16$ and $\alpha = 0.75$.

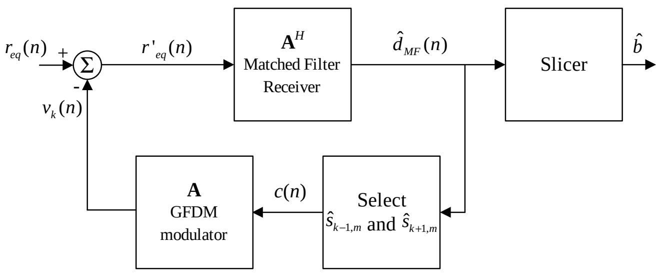

Fig. 8. Block diagram of the MFR-DSIC.

where $\mathbf{v_k}$ is the GFDM frame with the ICI present in the k-th subcarrier and $\mathbf{c}$ is the vector representation of (24).

A new version of the equalized received signal is obtained by

$$\mathbf{r}'_{\mathbf{eq}} = \mathbf{r}_{\mathbf{eq}} - \mathbf{v}_{\mathbf{k}}, \tag{26}$$

which has low ICI in the k-th subcarrier.

The signal obtained in (26) is used to eliminate the ICI from the next subcarrier and the process continues until the ICI is minimized for all subcarriers. The whole process can be repeated I times to achieve better results.

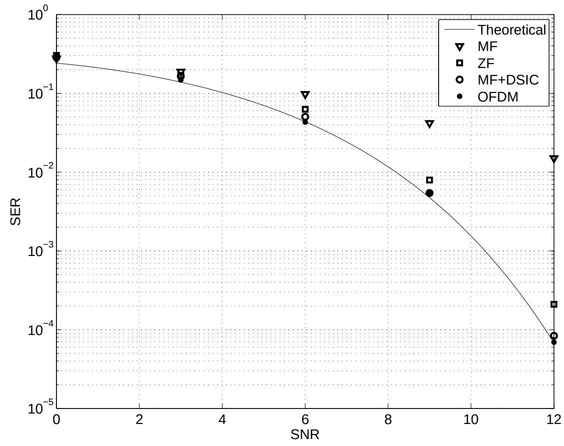

Fig. 9. SER for OFDM and GFDM over AWGN channel.

IV. Performance over AWGN channel

The comparison between GFDM and OFDM symbol error rates (SER) over AWGN channel is the first step for performance assessment. The symbol error probability of a J-QAM OFDM system over AWGN channel is approximately given by [15]

$$p_e \approx \frac{4(\sqrt{J}-1)}{\sqrt{J}} \mathrm{Q}\left(\sqrt{\frac{3\bar{E}}{(J-1)\,N_0}}\right), \tag{27}$$

where $\bar{E}$ is the average symbol energy of the constellation and N_0 is the noise power spectral density.

Figure 9 shows the symbol error rate of OFDM and GFDM over AWGN channel. The parameters used in the simulation are presented in Table I. ZFR, MFR and MFR-DSIC have been considered for reception of the GFDM signal.

TABELA I

Simulation parameters

Parameter	Value
Number of time-slots (M)	3
Number of subcarriers (K)	64
Upsampling Factor (N)	64
Duration of time-slot/OFDM symbol	256 μs
Subcarrier spacing	3,906 Hz
Constellation order (J)	4
Transmit Filter (GFDM)	RRC
Roll-off factor	0.5
Number os iterations for DSIC (I)	3

From Figure 9 it is possible to observe that the ICI causes the MFR to achieve the poorest performance. ZFR can eliminate the ICI and, therefore, it outperforms the MFR. However, one can notice from Figure 9 that the noise enhancement introduced by the ZFR reduces its performance in 0.6 dB, which tends to be an asymptotic loss. The MFR-DSIC is able to remove the ICI without introducing the noise enhancement and, therefore, it matches the theoretical performance over AWGN channel.

V. Performance over Frequency-Selective channels

The symbol error probability of OFDM over frequency-selective channels can be approximately given by [35]

$$p_{e_s} \approx \frac{4(\sqrt{J}-1)}{\sqrt{2\pi J}\,K} \sum_{k=0}^{K-1} \frac{\gamma_k}{1+\gamma_k^2} e^{-\frac{\gamma_k^2}{2}}, \tag{28}$$

where

$$\gamma_k = \sqrt{|H_k|^2 \frac{3\bar{E}}{(J-1)\,N_0}}, \tag{29}$$

and H_k is the channel gain in the frequency of the k-th subcarrier.

Table II lists the channel delay profiles that have been considered to evaluate the SER performance over frequency-selective channels. These channels typically represent the WRAN scenarios for IEEE 802.22 [32].

TABELA II

Delay profile used in simulations.

Channel A	Coherence bandwidth: 7.23 kHz					
Delay (μs)	0	3	8	11	13	21
Path Gain (dB)	0	-7	-15	-22	-24	-19
Channel B	Coherence bandwidth: 11.97 kHz					
Delay (μs)	0	2	3	4	7	11
Path Gain (dB)	0	-7	-6	-22	-16	-20
Channel C	Coherence bandwidth: 3.57 kHz					
Delay (μs)	0	2	5	16	24	33
Path Gain (dB)	0	-9	-19	-14	-24	-16
Channel D	Coherence bandwidth: 1.22 kHz					
Delay (μs)	0	2	5	16	22	60
Path Gain (dB)	0	-10	-22	-18	-21	-10

Comparing the coherence bandwidth of the channels presented in Table II with the subcarrier frequency spacing used in simulations, it is possible to conclude that channels C and D cannot be considered flat for a single subcarrier. It is important to observe that (28) does not hold in this case and the frequency-domain zero-forcing equalizer is not suitable for these channels.

Figure 10 shows the SER performance of OFDM and GFDM systems over channel A, while Figure 11 presents the SER performance over channel B. The first observation that can be made is that the channel frequency selectivity reduces the SER performance of both systems. Again, MFR has the poorest performance in both channels due to ICI. The ZFR also unveils a performance loss of about 0.6 dB when compared with theoretical curve and MFR-DSIC matches the performance of OFDM.

Figures 12 and 13 show the SER performance of OFDM and GFDM over channels C and D, respectively. As expected, the theoretical symbol error probability curve evaluated for OFDM is not valid when the channel coherence bandwidth is smaller than the bandwidth of each subcarrier. The mismatch between the simulation and theoretical results becomes clear in Figure 13, where the channel frequency selectivity is more severe.

It is also important to notice that GFDM with ZFR and MFR-DSIC have achieved approximately the same performance than OFDM over channel C (Figure 12), whereas

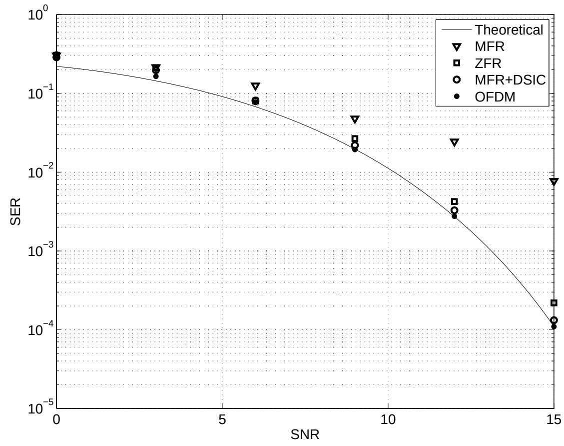

Fig. 10. SER for OFDM and GFDM over channel A.

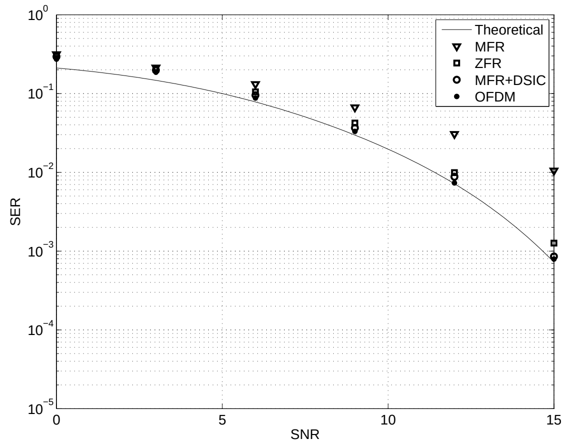

Fig. 11. SER for OFDM and GFDM over channel B.

it has outperformed OFDM over channel D (Figure 13). Complementary simulations have shown that the SER performance of GFDM with ZFR and MFR-DSIC over frequency-selective channels with small coherence bandwidth improves when the number os time-slots increases. This observation lets one to conclude that GFDM can achieve a better spectral resolution in the channel estimation because it uses M samples per subcarrier, while OFDM employs only one sample per subcarrier. Also, it is important to highlight that the results shown in this paper have been obtained with 4-QAM. High order modulation can lead to error propagation in the DSIC algorithm, decreasing the SER performance of the MFR-DSIC.

VI. Conclusions

CR is a technology that is being pointed out as a solution to mitigate the spectrum overcrowding, allowing for wireless broadband access in rural areas. Since incumbent users must be protect from interferences caused by secondary users, it is very important to CRs to reduce the out-of-band emissions and, therefore, GFDM is an interesting multi-carrier solution

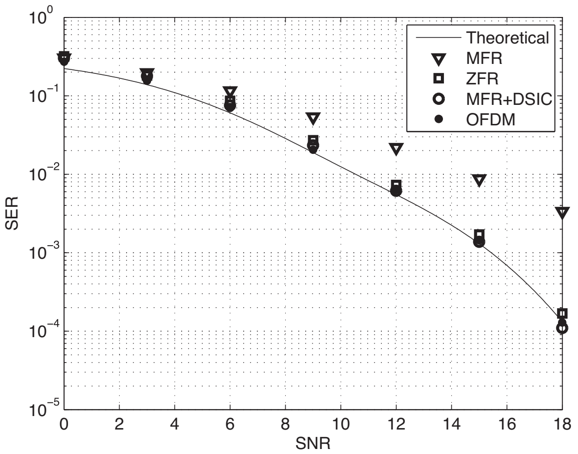

Fig. 12. SER for OFDM and GFDM over channel C.

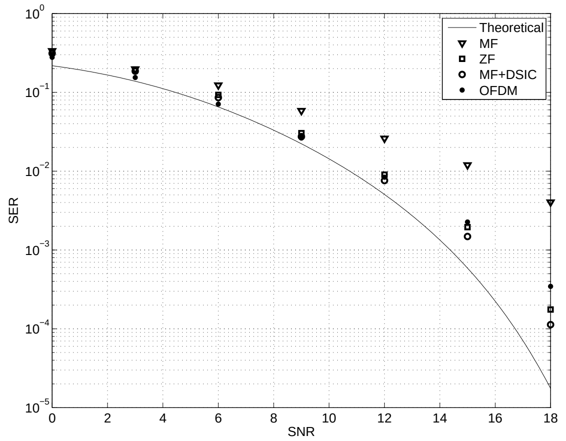

Fig. 13. SER for OFDM and GFDM over channel D.

for this application.

This paper has shown that GFDM matches OFDM performance over frequency-selective channels with coherence bandwidth larger than the bandwidth of each subcarrier, when MFR-DSIC is employed. This means that the theoretical SER estimation evaluated for OFDM can also be used to estimate the GFDM performance over frequency-selective channels. Another interesting observation is that GFDM outperforms OFDM when the channel coherence bandwidth is smaller than the bandwidth of each subcarrier. The main reason for this performance gain is the fact that GFDM has M samples available per frame to perform equalization, while OFDM has only one, which means that GFDM can achieve higher resolution and, consequently, a better performance. This performance gain cannot be observed in channels with high coherence bandwidth because the channel frequency response is practically flat for each subcarrier.

Simulation results have shown that ZFR unveils a performance loss that asymptotically tends to 0.6 dB when the channel coherence bandwidth is larger than the subcarriers' bandwidth. Although this is an initial observation and further investigation must take place, it is possible to conclude that the MFR-DSIC trade-off between complexity and performance may not be interesting when compared with ZFR, mainly in applications that requires low cost devices.

ACKNOWLEDGMENTS

The authors would like to thank Inatel for the financial support and Dipl.-Ing. Nicola Michailow and Prof. Dr.-Ing. Dr. h.c. Gerhard Fettweis for the technical support.

REFERÊNCIAS

[1] Donald Cox. Fundamental limitations on increasing data rate in wireless systems. *IEEE Communications Magazine*, 46(12):16–17, December 2008.

[2] Kate Harrison, Shridhar Mubaraq Mishra, and Anant Sahai. How much white-space capacity is there? In *Proceedings of IEEE Symposium on New Frontiers in Dynamic Spectrum*, pages 1–10, Singapore, April 2010. IEEE.

[3] Hamid Reza Karimi. Geolocation databases for white space devices in the UHF TV bands: Specification of maximum permitted emission levels. In *Proceedings of IEEE Symposium on New Frontiers in Dynamic Spectrum Access Networks*, pages 443–454, Aachen, Germany, May 2011. IEEE.

[4] P. Marshall. Analogue switch-off and its implications. In *Proceedings of The IEE Storage and Home Networks Seminar*, volume 2004, pages 108–116. IEE, 2004.

[5] Francois Rancy, Elmar Zilles, and Jean-Jacques Guitot. Transition to digital TV and digital dividend. pages 13–20. IEEE, October 2011.

[6] Huseyin Arslan. *Cognitive Radio, Software Defined Radio, and Adaptive Wireless Systems*. Springer, [New York], 2007.

[7] Joseph Mitola. Cognitive radio for flexible mobile multimedia communications. In *Proceeding of IEEE International Workshop on Mobile Multimedia Communications*, pages 3–10, San Diego, CA, USA, November 1999. IEEE.

[8] Carlos Cordeiro, Kiran Challapali, and Dagnachew Birru. IEEE 802.22: An introduction to the first wireless standard based on cognitive radios. *Journal of Communications*, 1(1), 2006.

[9] 802.16h-2010. Technical report, Institute of Electrical and Electronics Engineers, New Jersey, USA, July 2010.

[10] Hyunduk Kang, Donghun Lee, Byung-Jang Jeong, and Allen C. Kim. Coexistence between 802.22 and 802.11af over TV white space. In *Proceedings of International Conference on ICT Convergence*, pages 533–536, Seoul, South Korea, September 2011. IEEE.

[11] Xinsheng Zhao, Zhiyi Guo, and Qiang Guo. A cognitive based spectrum sharing scheme for LTE advanced systems. In *Proceedings of International Congress on Ultra Modern Telecommunications and Control Systems and Workshops*, pages 965–969, Moscow, Russia, October 2010. IEEE.

[12] Erik Axell, Geert Leus, Erik Larsson, and H. Poor. Spectrum sensing for cognitive radio : State-of-the-art and recent advances. *IEEE Signal Processing Magazine*, 29(3):101–116, May 2012.

[13] A. Ghasemi and E.S. Sousa. Spectrum sensing in cognitive radio networks: requirements, challenges and design trade-offs. *IEEE Communications Magazine*, 46(4):32–39, April 2008.

[14] Yonghong Zeng, Ying-Chang Liang, Anh Tuan Hoang, and Rui Zhang. A review on spectrum sensing for cognitive radio: Challenges and solutions. *EURASIP Journal on Advances in Signal Processing*, 2010:1–16, 2010.

[15] Ahmad R. S Bahai and Burton R Saltzberg. *Multi-carrier digital communications theory and applications of OFDM*. Kluwer Academic/Plenum, New York, 1999.

[16] Jaap Van De Beek and Fredrik Berggren. Out-of-band power suppression in OFDM. *IEEE Communications Letters*, 12(9):609–611, September 2008.

[17] Myonghee Park, Heeyoung Jun, Jaehee Cho, Namshin Cho, Daesik Hong, and Changeun Kang. PAPR reduction in OFDM transmission using hadamard transform. pages 430–433, New Orleans, LA, USA, April 2011.

[18] Xin chun Wu, Jin xiang Wang, and Zhi gang Mao. A novel PTS architecture for PAPR reduction of OFDM signals. In *2008 11th IEEE Singapore International Conference on Communication Systems*, pages 1055–1060, Guangzhou, China, November 2008.

[19] Benjamin Lee, Dilip V. Sarwate, and Douglas L. Jones. Peak to average power ratio reduction of an OFDM signal using a practical selective mapping approach with embedded side-information. In *2009 Conference Record of the Forty-Third Asilomar Conference on Signals, Systems and Computers*, pages 972–976, Pacific Grove, CA, USA, 2009.

[20] k. Yang and S. Chang. Peak to average power control in OFDM using standard arrays of linear block codes. *IEEE Communications Letters*, pages 174–176, April 2003.

[21] Enrique Mariano Lizarraga, Alexis Alfredo Dowhuszko, and Victor Hugo Sauchelli. Improving out-of-band power emissions in OFDM systems using double-length symbols. *IEEE Latin America Transactions*, 10(3):1710–1718, April 2012.

[22] Gerhard Fettweis, Marco Krondorf, and Steffen Bittner. GFDM - generalized frequency division multiplexing. pages 1–4. IEEE, April 2009.

[23] Nicola Michailow, Ivan Gaspar, Stefan Krone, Michael Lentmaier, and Gerhard Fettweis. Generalized frequency division multiplexing: Analysis of an alternative multi-carrier technique for next generation cellular systems. In *Proceedings of International Symposium on Wireless Communication Systems*, pages 171–175, Paris, France, August 2012. IEEE.

[24] Rohit Datta, Kamran Arshad, and Gerhard Fettweis. Analysis of spectrum sensing characteristics for cognitive radio GFDM signal. In *Proceedings of 8th International Wireless Communications and Mobile Computing Conference*, pages 356–359, Limassol, Chipre, August 2012. IEEE.

[25] Rohit Datta, Gerhard Fettweis, Yasunori Futatsugi, and Masayuki Ariyoshi. Comparative analysis on interference suppressive transmission schemes for white space radio access. In *Proceedings of IEEE 75th Vehicular Technology Conference (VTC Spring)*, pages 1–5, Yokohama, Japan, May 2012. IEEE.

[26] Nicola Michailow. *Integration of a GFDM Secondary System in an Existing OFDM System*. PhD thesis, Technische Universitat Dresden, Dresden, Germany, July 2010.

[27] Ahmad Bahai, Manonnet Singh, Andrea Goldsmith, and Burton Saltzberg. A new approach for evaluating clipping distortion in multicarrier systems. *IEEE Journal on Selected Areas in Communications*, 20, no 5(5):1037–1046, June 2002.

[28] Rohit Datta, Nicola Michailow, Michael Lentmaier, and Gerhard Fettweis. GFDM interference cancellation for flexible cognitive radio PHY design. In *Proceedings of the 76th IEEE Vehicular Technology Conference (VTC Fall'12)*, volume 1, QuÃ©bec City, Canada, September 2012. IEEE.

[29] Anderson Soares, Luciano Mendes, and Rausley Souza. Análise de desempenho do algoritmo de water-filling modificado para alocação de recursos em sistemas OFDMA. In *Anais do XXX Simpósio Brasileiro de Telecomunicações*, Brasília, Brasil, 2012. SBrT.

[30] Peiman Amini. *Filter Bank Multicarrier Techiniques for Cognitive Radios*. PhD thesis, University of Utah, Salt Lake City, USA, 2009.

[31] Ronald Schafer Alan Oppenheim. *Discrete-Time Signal Processing, 3rd Edition*. Prentice Hall, [New York], 2009.

[32] Hyunwook Kim, Jaewoon Kim, Suckchel Yang, Minki Hong, and Yoan Shin. An Effective MIMO OFDM System for IEEE 802.22 WRAN Channels. *IEEE Transactions on Circuits and Systems*, 55(8), August 2008.

[33] Bernad Sklar. *Digital Communications: Fundamentals and Applications*. Prentice Hall, New York, 2 edition, 2001.

[34] Nicola Michailow, Rohit Datta, Stefan Krone, Michael Lentmaier, and Gerhard Fettweis. Generalized frequency division multiplexing: A flexible multi-carrier modulation scheme for 5th generation cellular networks. In *Proceedings of the German Microwave Conference (GeMiC'12)*, Ilmenau, March 2012.

[35] Luciano Mendes and Renato Baldini Filho. Performance of WHT-STC-OFDM in Mobile Frequency Selective Channel. In *Proceedings of the International Telecommunication Symposium*, Manaus, 2010.

Bruno Moreira Alves was Born in Pindamonhangaba, SP, Brazil, on August 02, 1986. He holds the title as Electrical Engineer (Inatel, 2011). In 2011 he started a Master's degree at Inatel, studying physical interfaces for Cognitive Radio. Since 2011, he works with Digital Television at Hitachi Kokusai Linear in Santa Rita do Sapucaí.

Luciano Leonel Mendes was Born in São José dos Campos, SP, Brazil, on August 29, 1977. He holds the titles: Electronics Technician (ETEP, 1996), Electrical Engineer (Inatel, 2001), Master in Telecommunication (Inatel, 2003) and Doctor in Electrical Engineering (Unicamp, 2007). Since 2001 he is Professor at Inatel where he is the Technical Manager of the Hardware Development Laboratory and Coordinator of the Master in Telecommunications program. He has also coordinated several projects funded by FAPEMIG, FINEP and BNDES. He is member of the Technical Program Committee of the Brazilian Telecommunication Society (SBrT) and Technical chairman of International Workshop on Telecommunications. His main area of research is broadband wireless communication and currently he is working on multicarrier modulation for Cognitive Radios.

Dayan Adionel Guimarães was Born in Carrancas, MG, Brazil, on March 01, 1969. He holds the titles: Electronics Technician (ETE FMC, 1987), Electrical Engineer (Inatel, 1994), Specialist in Data Communication Engineering (Inatel, 2003), Specialist in Human Resources Management (FAI, 1996), Master in Electrical Engineering (Unicamp, 1998) and Doctor in Electrical Engineering (Unicamp, 2003). In 2010 he attended a Pos-Doctoral internship at Federal University of Santa Catarina (UFSC), studying Spectrum Sensing for Cognitive Radio applications and Convex Optimization. From 1988 to 1993 he developed equipment for Industrial Instrumentation and Control, and also occupied the positions of Manufacturing and Product Engineering Supervisor at SENSE Sensores e Instrumentos. Since January 1995 he is Professor at Inatel where, for eight years, he was responsible for the structure that supports practical teaching activities for the Electrical Engineering undergraduate course. His research includes the general aspects of Digital Transmission and Mobile Communications. He is currently working on Eigenvalue-Based Spectrum Sensing for Cognitive Radio. Dr. Dayan is member of the Telecomunicações magazine's Editorial Board, member of the Inatel's Master Degree Counseling Board and of the IEICE (Institute of Electronics, Information and Communication Engineers), Japan.

Ivan Simões Gaspar received the degree of Electrical Engineer and M.Sc. in Telecommunications from INATEL (National Institute of Telecommunications in Brazil), in 2003 and 2006 respectively. Also hold a certificate as Electronic Technician from the Technical School of Electronics "Francisco Moreira da Costa" in 1998. From 2003 to 2011 he was as technical supervisor and product manager in the department of research and development of Linear Electronic Equipment SA (now part of Hitachi Kokusai Electric Inc.) and worked on the design of new technological systems for TV broadcasting employing FPGA. From 2008 to 2011 he collaborated as an auxiliary lecturer at INATEL. Since February 2012 he is a research associate at the Vodafone Chair / TU Dresden working on Robust Non-Orthogonal Modulation schemes for 5G Cellular, specifically heading the demonstration work package on 5GNOW (EU FP7 project) and software defined radio implementation activities on the RF Lead User Program with National Instruments.